

# New Demodulation Method for Efficient Phase-Rotation-Based Beamforming

Anup Agarwal, *Student Member, IEEE*, Yang Mo Yoo, *Student Member, IEEE*,  
Fabio Kurt Schneider, *Student Member, IEEE*, Changqing Gao, Liang Mong Koh,  
and Yongmin Kim, *Fellow, IEEE*

**Abstract**—In this paper, we present a new demodulation method to reduce hardware complexity in phase-rotation-based beamforming. Due to its low sensitivity to phase delay errors, quadrature demodulation, which consists of mixing and lowpass filtering, is commonly used in ultrasound machines. However, because it requires two lowpass filters for each channel to remove harmonics after mixing, the direct use of quadrature demodulation is computationally expensive. To alleviate the high computational requirement in quadrature demodulation, we have developed a two-stage demodulation technique in which dynamic receive focusing is performed on the mixed signal instead of the complex baseband signal. Harmonics then are suppressed by using only two lowpass filters. When the number of channels is 32, the proposed two-stage demodulation reduces the necessary number of multiplications and additions for phase-rotation beamforming by 82.7% and 88.2%, respectively, compared to using quadrature demodulation. We have found from simulation and phantom studies that the proposed method does not incur any significant degradation in image quality in terms of axial and lateral resolution. These preliminary results indicate that the proposed two-stage demodulation method could contribute to significantly reducing the hardware complexity in phase-rotation-based beamforming while providing comparable image quality.

## I. INTRODUCTION

THE adoption of digital receive beamforming (DRBF) in medical ultrasound imaging systems based on dynamic focusing has greatly improved the image quality in the last few decades [1]. In the DRBF, the enhanced time-delay accuracy in digital processing results in high signal-to-noise ratio (SNR) and spatial resolution [2]. However, the DRBF significantly increases the computational complexity because it requires fast analog-to-digital converters (ADCs) and front-end digital circuitries running at a high clock frequency. To alleviate the high-frequency sampling requirement in ADCs, interpolation beamforming (IBF) and phase-rotation-based beamforming (PRBF) with quadrature demodulation (QD) have been developed [2]–[4], and they are commonly used in ultrasound machines [5]. Although the developed IBF and PRBF re-

duce the hardware complexity in high-speed ADCs, they require multiple computationally-expensive finite-impulse response (FIR) filters (i.e., interpolation and demodulation filters for the IBF and QD-based PRBF, respectively). Thus, this high computational requirement makes development of ultrasound machines with large channel counts [e.g., for three-dimensional (3-D) ultrasound systems [6]] or very low-end machines (e.g., handheld [7]) challenging.

For further reduction in the hardware burden for the DRBF, various beamforming methods, such as pipelined-sampled-delay-focusing (PSDF) [8], sigma-delta oversampled [5], and direct in-phase/quadrature (I/Q) [9], have been developed. In the PSDF technique, nonuniform sampling of the signals received from different channels is performed to achieve dynamic focusing without the need of the complicated digital delay circuitries (i.e., interpolation or phase rotation). However, the control of ADCs for nonuniform sampling is complicated [10]. The sigma-delta oversampled beamforming techniques also eliminate the need of interpolation or phase rotation by using one-bit, sigma-delta modulators running at a high clock frequency, but they suffer from artifacts caused by asynchronism between the sigma-delta modulator at each channel and the post-beamforming demodulator [5], [11], [12]. Furthermore, developing sigma-delta modulators that can provide the required sensitivity (in terms of signal-to-quantization noise ratio) for supporting various medical ultrasound applications remains challenging [5]. In the direct I/Q method [9], the complex baseband signals used in the PRBF are directly sampled from the receive signals, but this method introduces image artifacts as it assumes narrow-band signals and no frequency-dependent attenuation, which are typically not satisfied in medical ultrasound imaging.

In this paper, we propose a new demodulation method (i.e., two-stage demodulation) for the efficient PRBF. In the developed method, coherent summation for dynamic receive focusing is performed on the mixed signal instead of the complex baseband signal, then harmonics are suppressed after dynamic receive focusing by using only two lowpass filters.

## II. THEORY

### A. PRBF with Quadrature Demodulation

Fig. 1 shows the block diagram of the PRBF with quadrature demodulation, which consists of mixing and

Manuscript received January 30, 2006; accepted March 27, 2007.

A. Agarwal, Y. M. Yoo, F. K. Schneider, and Y. Kim are with the Image Computing Systems Laboratory, Departments of Electrical Engineering and Bioengineering, University of Washington, Seattle, WA 98195-5061 (e-mail: ykim@u.washington.edu).

C. Gao and L. M. Koh are with the School of Electrical and Electronic Engineering, Nanyang Technological University, Singapore 639798.

Digital Object Identifier 10.1109/TUFFC.2007.437

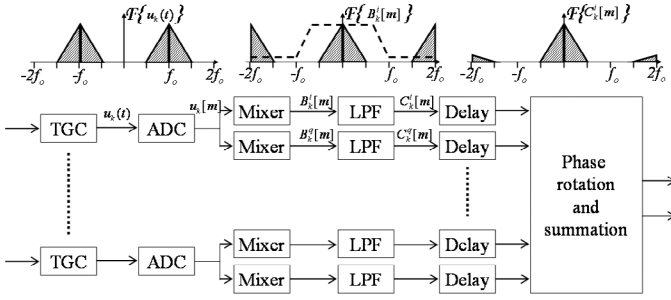


Fig. 1. Block diagram of the QD-based PRBF when  $f_{\text{adc}} = 4f_0$ .  $F\{\bullet\}$  represents the Fourier transform.

lowpass filtering. The received ultrasound signals coming from transducer elements are centered around  $\pm f_0$  where  $f_0$  is the transducer center frequency. These signals are amplified in proportion to depth in order to compensate for signal attenuation [i.e., time-gain compensation (TGC)]. After TGC, the RF signals are digitized by ADCs, whose sampling frequency ( $f_{\text{adc}}$ ) is typically  $4f_0$ . The digitized RF signal for the  $k^{\text{th}}$  channel is represented by [13], [14]:

$$\begin{aligned} u_k[m] &= A_k^i[m] \cos[\omega_0 m] - A_k^q[m] \sin[\omega_0 m], \\ m &= 1, 2, \dots, M \text{ and } k = -K/2, \dots, K/2 - 1, \end{aligned} \quad (1)$$

where  $\omega_0 = 2\pi f_0$ ,  $M$  is the number of samples per scanline,  $K$  is the number of receive channels, and  $A_k^i$  and  $A_k^q$  are the in-phase and quadrature baseband signal component, respectively.

The baseband signals can be extracted by removing the carrier frequency through QD. In QD, the digitized RF signal (i.e.,  $u_k[m]$ ), which is originally centered around  $\pm f_0$ , is first multiplied with cosine ( $\cos[\omega_0 m]$ ) and sine ( $\sin[\omega_0 m]$ ) values. These multiplications generate not only the signals centered at 0, but also signal harmonics centered at  $\pm 2f_0$  in the in-phase and quadrature components of the mixed signal (i.e.,  $B_k^i[m]$  and  $B_k^q[m]$ , respectively). To remove these replicas and obtain the complex baseband signal, lowpass filtering is performed after mixing. This demodulation filtering introduces a significant computational burden on the PRBF [9]. Phase rotation and summation (i.e., dynamic receive focusing) are performed on the delayed complex baseband signals. Because dynamic receive focusing is performed on baseband signals, the beamforming frequency ( $f_{\text{bf}}$ ) could be lower than the ADC sampling frequency, i.e.,  $f_{\text{bf}} = f_{\text{adc}}/\eta$  when  $\eta > 1$ , where  $\eta$  is the ratio of the ADC sampling frequency to the beamforming frequency. However, reducing  $f_{\text{bf}}$  could introduce signal aliasing when  $f_{\text{bf}}$  is lower than the bandwidth (BW) of the complex baseband signal [15]. Thus,  $f_{\text{bf}}$  in the QD-based PRBF must be greater than or equal to BW to avoid signal aliasing.

### B. PRBF with Two-Stage Demodulation

To reduce the complexity of demodulation filtering in the PRBF, we developed a new demodulation method called two-stage demodulation (TSD), in which QD is per-

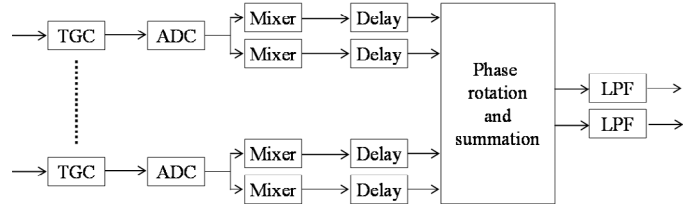


Fig. 2. Block diagram of the TSD-based PRBF.

formed in two stages. Although mixing is performed before dynamic receive focusing, the more computationally-expensive demodulation filtering is performed after dynamic receive focusing. Fig. 2 shows the block diagram of the TSD-based PRBF, which reduces the number of lowpass filters by a factor equal to the number of receive channels. Thus, the proposed demodulation method could significantly reduce the computational requirement for the DRBF. However, it could suffer from artifacts due to non-linearity in dynamic receive focusing and signal aliasing when  $f_{\text{bf}} < f_{\text{adc}}$  due to the presence of signal harmonics at  $\pm 2f_0$  during dynamic receive focusing.

Dynamic focusing is effectively equivalent to nonuniform sampling along the scanline (i.e., different depths are delayed by different amounts). Thus, the TSD-based PRBF could introduce artifacts because demodulation filtering is performed on nonuniformly sampled data. Similar errors were reported for the sigma-delta oversampled beamforming methods [5] and the post-compression-based coded excitation beamforming methods [16]. To analyze the error in the TSD due to dynamic focusing, we have derived the expression for the final beamformed signal in the Appendix when the PRBF is performed with QD and TSD. In the TSD-based PRBF, dynamic focusing introduces an error in sample selection during demodulation filtering, i.e., sample selection error (SSE). The expression for the SSE has been derived in the Appendix [i.e., (A13)] and is given by:

$$\text{SSE}(m, j, k, \eta) = \Delta[m, k] - \Delta[m + \eta j, k], \quad (2)$$

where  $j$  varies from  $-J/2$  to  $J/2 - 1$ ,  $J$  is the filter tap size, and  $\Delta[m, k]$  is the dynamic focusing delay applied to compensate for the delay difference between the  $k^{\text{th}}$  and center element in the ultrasound transducer. We have studied the magnitude of SSE as a function of the axial distance and evaluated the impact of SSE on image quality via simulation and phantom studies.

In addition to the SSE, the TSD-based PRBF could incur artifacts due to signal aliasing when  $f_{\text{bf}} < f_{\text{adc}}$  because of the presence of signal harmonics at  $\pm 2f_0$  during dynamic receive focusing. Using the bandpass sampling principle [17], we can derive the beamforming frequency ranges that can avoid signal aliasing in the TSD-based PRBF as follows:

$$f_{\text{bf}} > 2 \times (f_0 + BW/2), \quad (3)$$

$$f_0 + BW/2 < f_{\text{bf}} < 2 \times (f_0 - BW/2). \quad (4)$$

From (3) and (4),  $f_{\text{bf}} \geq 3f_0$  is required to avoid signal aliasing for  $\text{BW} \geq f_0$ , which is typical in B-mode ultrasound imaging. For example, the TSD-based PRBF would cause signal aliasing for  $\eta = 2, 3$ , and 4 when  $f_{\text{adc}} = 4f_0$  and  $\text{BW} = f_0$ . We have studied the effect of this signal aliasing on image quality via simulation and phantom studies.

### III. SIMULATION AND EXPERIMENTAL SETUP

#### A. SSE Analysis

A simulation model was developed in Matlab (The MathWorks Inc., Natick, MA) to emulate the SSE in the TSD-based PRBF. The magnitude of SSE was obtained as a function of the axial distance for 32/48/64-element linear array transducers with the transducer center frequency ( $f_0$ ) varying from 3.5 MHz to 7.5 MHz. The pitch was set to  $\lambda$  mm, where  $\lambda = c/f_0$  and  $c$  is the speed of sound. All the elements were used for dynamic receive focusing. An ADC sampling frequency of  $4f_0$  and  $\eta = 1, 2, 3$ , and 4 were used. Impact of dynamic receive aperture [2] on the magnitude of SSE also was evaluated by using  $f$ -number of 1.5 during receive beamforming.

#### B. Simulation and Phantom Studies for Image Quality Evaluation

1. *Simulation Study Setup:* Simulation was performed using the Field II [18] to compare the TSD-based PRBF with the QD-based PRBF in terms of spatial (i.e., axial and lateral) resolution. The transducer model used in simulation was an 82-element linear array transducer with  $f_0 = 3.5/5.5/7.5$  MHz and the  $-45$  dB bandwidth of  $1.4f_0$ . The pitch was  $\lambda$  mm, the element height was 14 mm, and the elevational focal point was 40 mm. 32- and 64-element apertures were used for transmission and reception of ultrasound signals with a transmit focus of 40 mm. Dynamic focusing and dynamic aperture with  $f$ -number of 1.5 were used during receive beamforming. An ADC sampling frequency of  $4f_0$  was used. To investigate the spatial resolution, a wire phantom was simulated with the wire locations determined by the SSE analysis results.

2. *Phantom Study Setup:* For the phantom study, a tissue mimicking phantom was used (Model 539 Multipurpose Phantom, ATS Laboratories Inc., Bridgeport, CT). A commercial ultrasound machine (SA-9900, Medison Corp., Seoul, Korea) was modified to acquire the prebeamformed data. A 192-element convex array transducer with a radius of 40 mm and a pitch of 0.31 mm was used. The transducer center frequency was 3.5 MHz, and the  $-45$  dB bandwidth was  $1.4f_0$ . A 64-element aperture was used for transmission and reception of the ultrasound signals, and the receive signal was quantized using 8-bit ADCs running at 15.4 MHz ( $4.4f_0$ ). Spatial resolution was evaluated using the wire targets, and the contrast resolution (CR) was measured for the cyst regions by:

TABLE I  
PARAMETERS USED IN SIMULATION AND PHANTOM STUDIES.

Parameter	Simulation	Phantom
Speed of sound (m/s)	1540	1450
Transducer type	linear	convex
Transducer center frequency (MHz)	3.5/5.5/7.5	3.5
Receive signal bandwidth ( $-45$ dB)	$1.4f_0$	$1.4f_0$
Sampling frequency (MHz)	$4f_0$	15.4
Transmit focus (mm)	40	50
Receive focus	dynamic	dynamic
Apodization	uniform	uniform
Number of scanlines	27	192
ADC quantization (bits)	8	8

$$\text{CR} = 1 - \frac{I_c}{I_s}, \quad (5)$$

where  $I_c$  and  $I_s$  are the average intensity inside cyst and speckle regions at the same depth, respectively [19]. Table I summarizes the various parameters used during simulation and phantom studies.

#### C. Computational Complexity Analysis

The computational complexity of each processing function in the QD- and TSD-based PRBF to generate one scanline data with  $K$  receive channels,  $J$ -tap demodulation filters,  $M$  ADC samples per scanline, and  $\eta$  (a ratio of the ADC sampling frequency to the beamforming frequency) was estimated in terms of 8-bit multiplications and additions required. The total number of multiplications and additions needed to support the QD- and TSD-based PRBF was derived for  $K = 32$ ,  $J = 16$ ,  $M = 4096$ , and  $\eta = 1, 2, 3$ , and 4.

## IV. RESULTS AND DISCUSSION

#### A. SSE Analysis

Fig. 3 shows the maximum value of the SSE as a function of the axial distance. As shown in Fig. 3, the SSE is large at depths closer to the transducer and decreases exponentially as the imaging depth is increased. Similarly, the impact of a nonunity  $\eta$  on the SSE decreases as the axial distance increases. For example, as  $\eta$  increases from 1 to 4, the SSE at the imaging depth of 5 mm increases from  $0.242 \mu\text{s}$  to  $0.813 \mu\text{s}$ , and that at the imaging depth of 20 mm increases from  $0.063 \mu\text{s}$  to  $0.146 \mu\text{s}$ .

Fig. 4 shows the maximum SSE as a function of the axial distance when the number of receive channels is varied. As shown in Fig. 4, there is an increase in the SSE magnitude as the number of channels increases. Fig. 5 shows the impact of increasing the transducer center frequency from 3.5 MHz to 7.5 MHz on the SSE in that increasing the transducer center frequency results in the reduction of the magnitude of SSE at all depths. This is because increasing  $f_0$  decreases the transducer pitch (i.e.,  $\lambda$ ), which reduces the SSE.

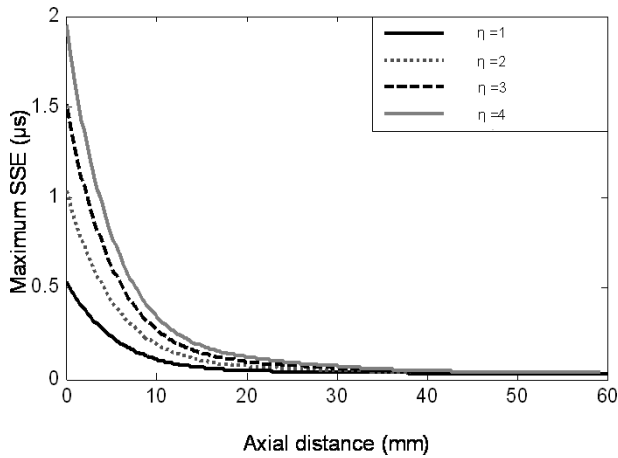


Fig. 3. Error in sample selection (in  $\mu\text{s}$ ) during demodulation filtering in the TSD-based PRBF.

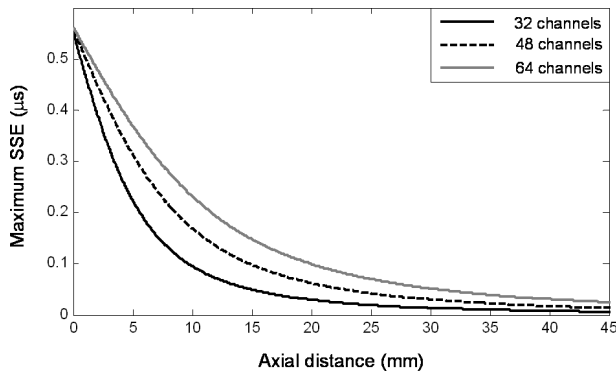


Fig. 4. Error in sample selection (in  $\mu\text{s}$ ) during demodulation filtering in the TSD-based PRBF for different receive channels.

The magnitude of the SSE can be further reduced by using a dynamic aperture technique during receive beamforming, which progressively increases the size of the receive aperture with increased imaging depth [2]. Fig. 6(a) shows the maximum SSE as a function of the axial distance when a dynamic aperture with  $f$ -number of 1.5 is used during receive beamforming for various values of  $\eta$ . Fig. 6(b) clearly shows the impact of dynamic aperture on SSE for  $\eta = 1$ . As shown in Figs. 6(a) and (b), the dynamic receive aperture technique significantly reduces the SSE at depths closer to the transducer (i.e., for the imaging depth of 5 mm, the maximum SSE is reduced from  $0.242 \mu\text{s}$  to  $0.025 \mu\text{s}$  and from  $0.813 \mu\text{s}$  to  $0.088 \mu\text{s}$  for  $\eta$  of 1 and 4, respectively). The impact of dynamic aperture on the maximum SSE diminishes with increasing depth. Furthermore, due to the depth-dependent receive aperture size and the  $f$ -number used, the maximum SSE value occurs at the depth of 17.9 mm. Similar results also have been obtained when the number of transducer channels is increased to 64 and dynamic aperture with  $f$ -number of 1.5 is used. The maximum SSE now occurs at an axial distance of 41 mm for  $\eta$  of 1. The impact of the SSE on the point spread function (i.e., axial and spatial resolution)

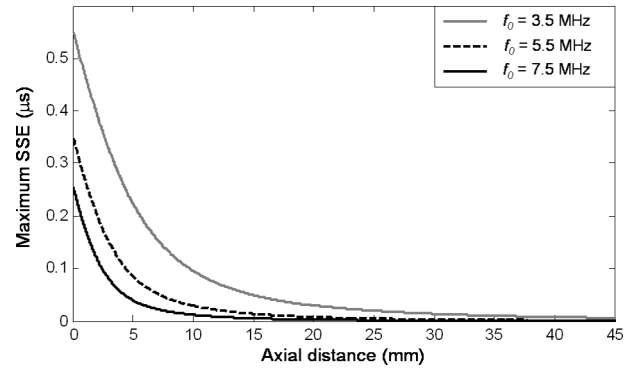


Fig. 5. Error in sample selection (in  $\mu\text{s}$ ) during demodulation filtering in the TSD-based PRBF for different transducer center frequencies.

was evaluated close to these imaging depths for 32- and 64-channel transducers.

### B. Image Quality Evaluation

1. *PRBF With TSD when  $\eta = 1$* : Fig. 7 shows the frequency spectrum, point spread function and the corresponding lateral and axial resolution for the wire target placed at the imaging depth of 18 mm when the PRBF is performed with the QD and TSD using 32 receive channels with a transducer center frequency of 3.5 MHz. As shown in Fig. 7(a), the harmonics present near  $\pm 2f_0$  in the output after summation in the TSD-based PRBF are removed during demodulation filtering. Thus, a frequency spectrum comparable to the QD-based PRBF is obtained after demodulation filtering in the TSD-based PRBF. As shown in Figs. 7(b) and (c), no significant difference is found with the TSD compared to the QD for both the axial and lateral resolution. No significant difference was found between the two methods for other imaging depths either. The impact of increasing the transducer center frequency on the spatial resolution with the TSD-based PRBF was evaluated using  $f_0$  of 5.5 MHz and 7.5 MHz, respectively. Fig. 8 shows the lateral and axial resolution using the QD- and TSD-based PRBF for the wire target placed at the imaging depth of 18 mm for these two transducer center frequencies. As shown in Fig. 8, the TSD-based PRBF provides comparable lateral and axial resolution to that of the QD-based PRBF as the transducer center frequency increases. Similar results were obtained with other imaging depths. Fig. 9 shows the point spread function and the corresponding lateral and axial resolution for the wire target placed at the imaging depth of 41 mm when the number of channels is 64. As shown in Figs. 9(b) and (c), there is no significant difference between the TSD- and QD-based PRBF in terms of axial and lateral resolution.

The images from the tissue mimicking phantom beamformed using the QD- and TSD-based PRBF with a dynamic range of 60 dB are shown in Fig. 10. The image quality from both methods is comparable. For quantitative comparison, while the frequency spectrum and point spread function were evaluated at the imaging depths of 20 mm and 40 mm, the CR [based on (5)] was measured

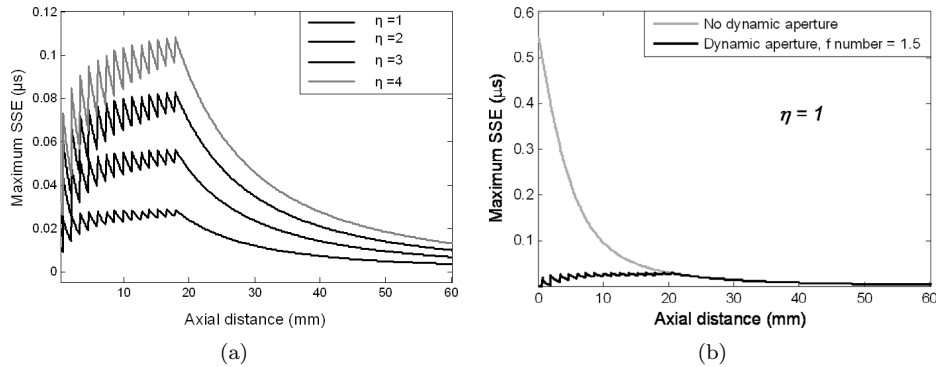


Fig. 6. (a) Error in sample selection (in  $\mu\text{s}$ ) during demodulation filtering in the TSD-based PRBF with dynamic aperture. (b) Comparison of SSE with and without dynamic aperture for  $\eta = 1$ .

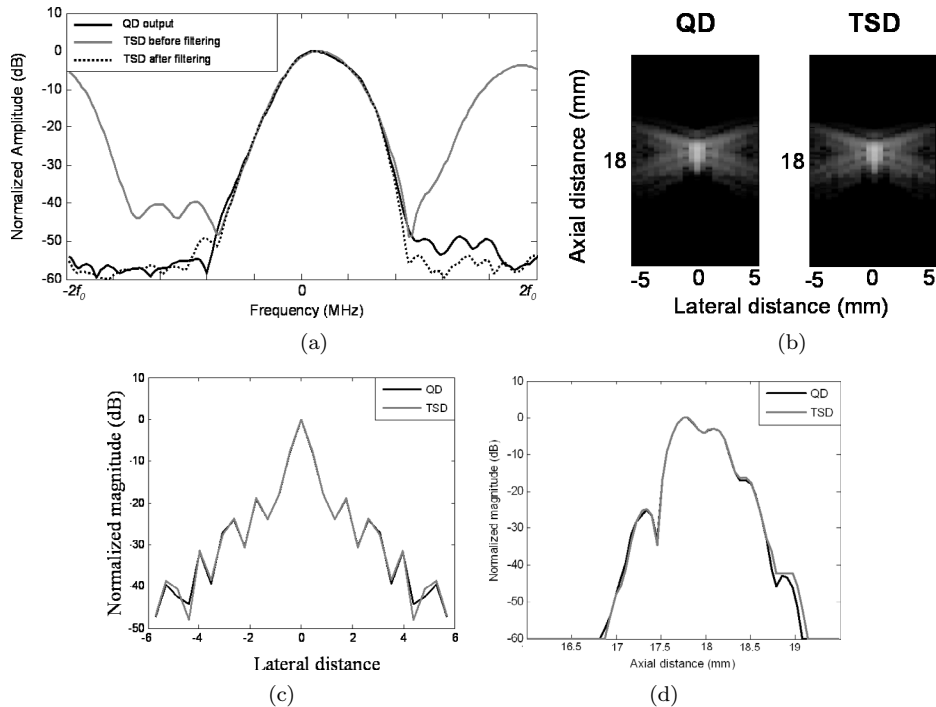


Fig. 7. Simulation results at the imaging depth of 18 mm for the 32-channel transducer. (a) Frequency spectrum. (b) Point spread function. (c) Lateral and (d) axial resolution for the QD- and TSD-based PRBF.

for the cyst region located at the depth of 40 mm [outlined with the dotted circle in Fig. 10(a)]. Figs. 11(a) and (d) show the frequency spectrum of the final output with the TSD- and QD-based PRBF when the imaging depth is 20 mm and 40 mm, respectively. As seen in Fig. 11, demodulation filtering in the TSD-based PRBF removes the harmonics near  $\pm 2f_0$  and there is no noticeable difference in the frequency spectrum between the TSD- and QD-based PRBF. Fig. 11 also shows the lateral and axial resolution using both methods. No perceptible difference is observed between the two methods, which is consistent with the simulation results. Table II shows the CR value obtained with the two methods. No significant difference (i.e.,  $< 0.3\%$ ) in the CR can be found. From the simulation and phantom studies, the TSD method has a negligible impact on image quality when  $f_{\text{bf}}$  is equal to  $f_{\text{adc}}$  (i.e.,  $\eta = 1$ ).

TABLE II  
CONTRAST RESOLUTION WITH THE QD-BASED PRBF AND THE TSD-BASED PRBF.

Method	CR
QD-based PRBF	0.751
TSD-based PRBF	0.749

2. *PRBF with TSD when  $\eta > 1$* : For  $\eta > 1$ , the TSD-based PRBF could introduce signal aliasing in addition to SSE. Fig. 12 shows the lateral and axial resolution obtained at the depth of 18 mm when the TSD-based PRBF is performed. As shown in Fig. 12(a), the side-lobe amplitude in the lateral direction is increased by about 10 dB with the TSD-based PRBF for  $\eta$  of 2 and 4. However, no significant degradation in the lateral resolution is observed

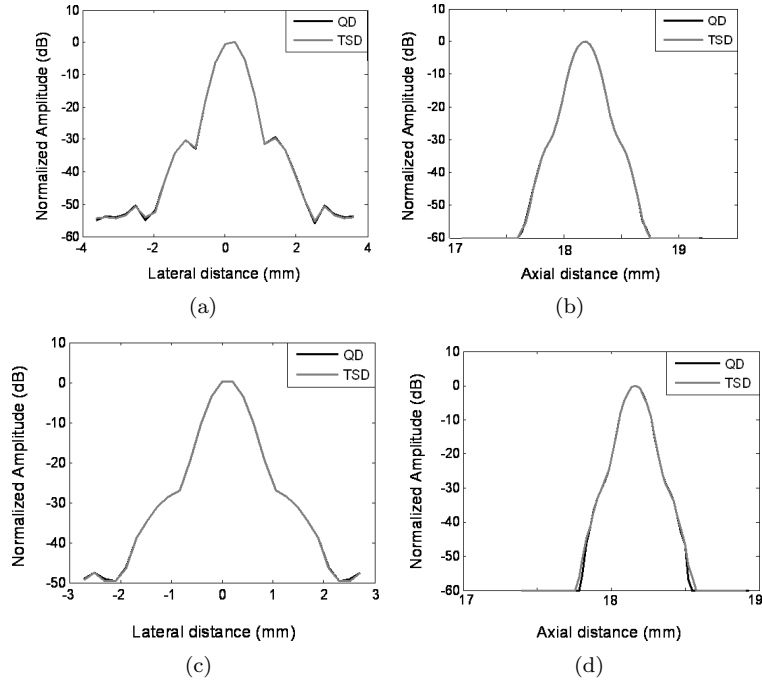


Fig. 8. Simulation results at the imaging depth of 18 mm with the QD- and TSD-based PRBF. (a) Lateral and (b) axial resolution for the transducer center frequency of 5.5 MHz. (c) Lateral and (d) axial resolution for the transducer center frequency of 7.5 MHz.

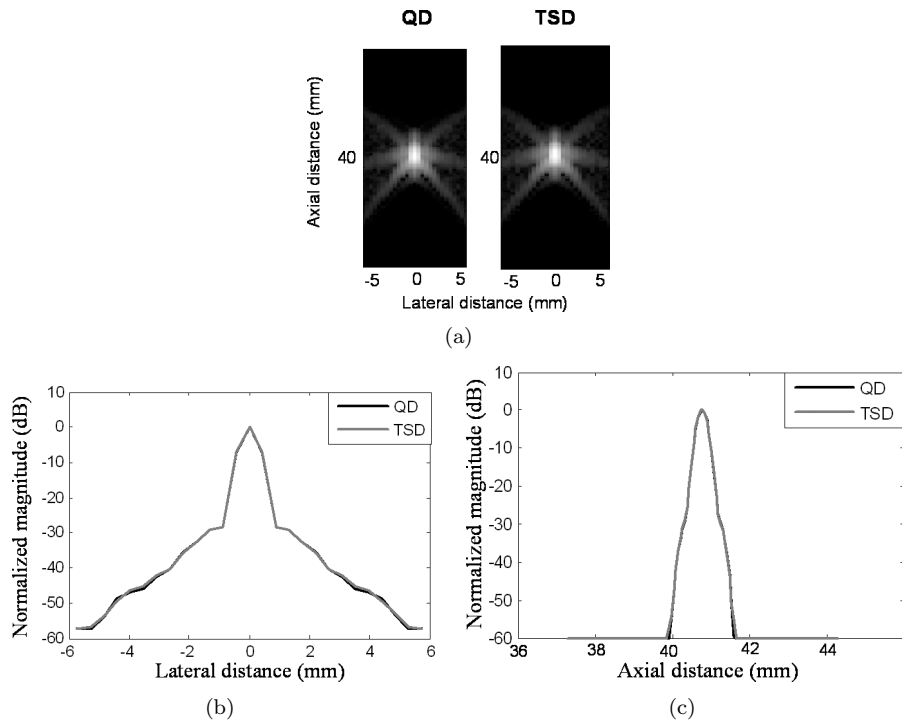


Fig. 9. Simulation results at the imaging depth of 40 mm for the 64-channel transducer. (a) Point spread function. (b) Lateral and (c) axial resolution for the QD- and TSD-based PRBF.

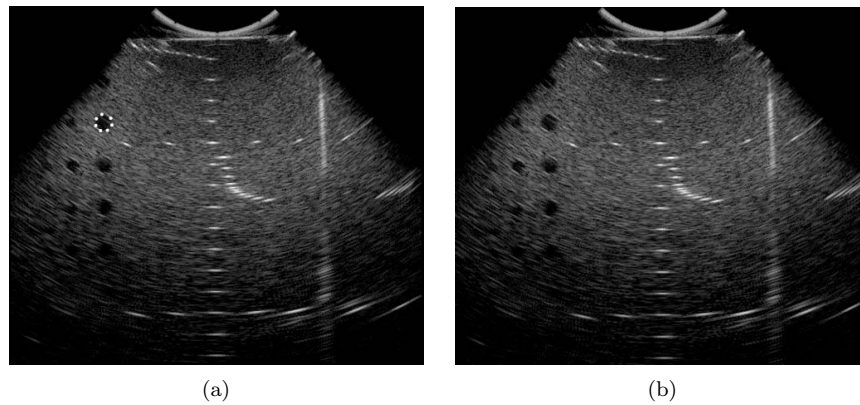


Fig. 10. Phantom study results with 60 dB dynamic range. Ultrasound images using (a) the QD-based PRBF and (b) the TSD-based PRBF. The cyst area at the depth of 40 mm is outlined with a dotted circle in (a).

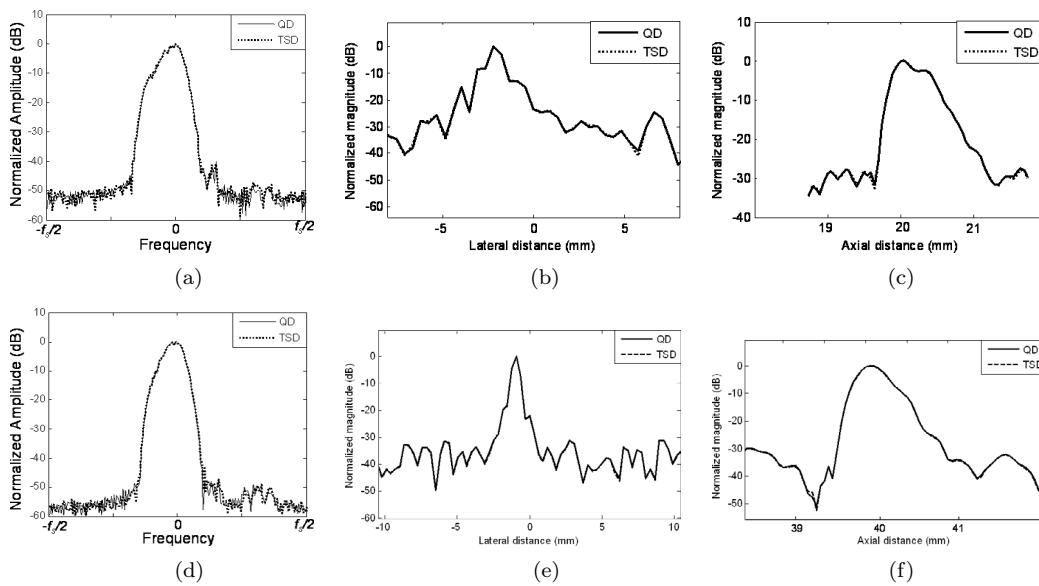


Fig. 11. Phantom study results with the QD- and TSD-based PRBF. (a) Frequency spectrum. (b) Lateral and (c) axial resolution at the imaging depth of 20 mm. (d) Frequency spectrum. (e) Lateral and (f) axial resolution at the imaging depth of 40 mm.

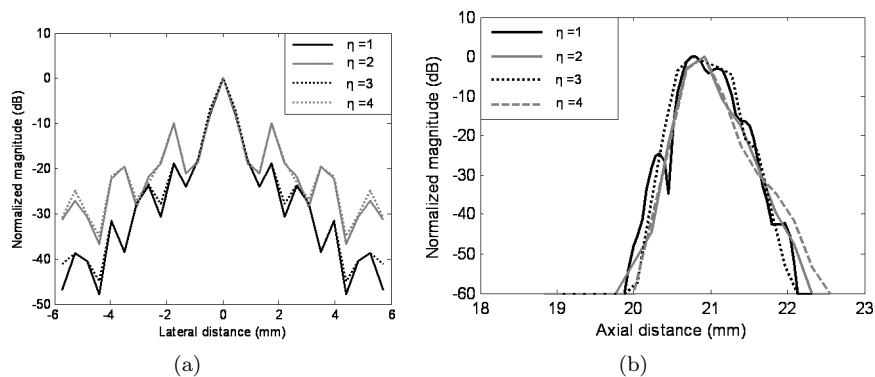


Fig. 12. Simulation results at the imaging depth of 18 mm at  $\eta$  of 1 to 4 in the TSD-based PRBF. (a) Lateral resolution. (b) Axial resolution.

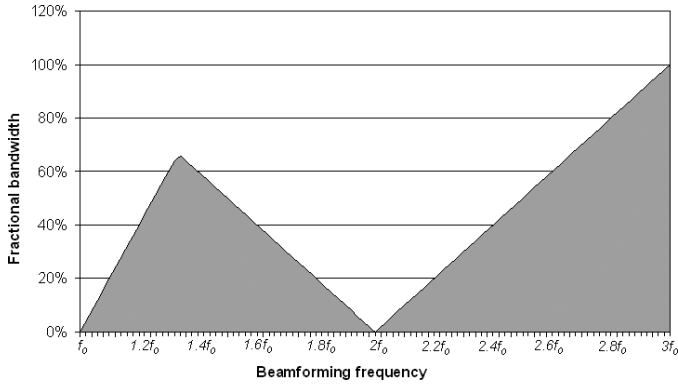


Fig. 13. Receive signal bandwidth that can be supported without signal aliasing as a function of the beamforming frequency in the TSD-based PRBF.  $f_0$  is the transducer center frequency.

when  $\eta$  is 3. For the axial resolution, there seems to be a small degradation with different values of  $\eta$  as shown in Fig. 12(b).

The superior performance of the TSD-based PRBF at  $\eta$  of 3 over  $\eta$  of 2 and 4 is due to signal aliasing. Fig. 13 shows, based on (3) and (4), the signal bandwidth that can be supported without signal aliasing for different beamforming frequencies in the TSD-based PRBF. As shown in Fig. 13, there is aliasing at the beamforming frequency of  $2f_0$  ( $\eta = 2$ ) and  $f_0$  ( $\eta = 4$ ) for any signal bandwidth, resulting in an increase in side-lobe energy. This is due to wrapping around of the signal harmonics originally centered at  $2f_0$  and  $-2f_0$  to the baseband (i.e., 0) due to these beamforming frequencies. This is illustrated in Figs. 14(a) and (b) that show the spectrum of the beamformed signal when the beamforming frequency is  $4f_0$  and  $2f_0$  ( $\eta$  is 2), respectively. However, for  $f_{bf} = 1.33f_0$  (i.e.,  $\eta$  is 3 when  $f_{adc}$  is  $4f_0$ ), the harmonics originally centered at  $2f_0$  and  $-2f_0$  wrap around to be centered at the frequencies of  $-0.67f_0$  and  $0.67f_0$ , respectively, as shown in Fig. 14(c). Thus, a receive signal with  $BW \leq 0.66f_0$  would not suffer from signal aliasing. For  $BW > 0.66f_0$ , there will be some aliasing when  $\eta$  is 3, but it would be less than when  $\eta$  is 2 or 4.

Fig. 15(a) shows the image of the tissue mimicking phantom obtained with the TSD-based PRBF when  $\eta$  is 3 (i.e.,  $f_{bf} = 1.33f_0$ ). For quantitative comparison, Figs. 15(b) and (c) show the lateral and axial resolution when  $\eta$  is 1 and 3. We can observe a slight axial and lateral resolution degradation when  $\eta$  is increased from 1 to 3. The CR was computed for the cyst marked in Fig. 10(a). As expected from Fig. 13, a reduced CR value of 0.737 with  $\eta$  of 3 was obtained compared to 0.749 with  $\eta$  of 1 due to signal aliasing because the BW of the receive signal in the phantom study was approximately  $1.4f_0$ . These preliminary results indicate that the proposed TSD-based PRBF with a nonunity  $\eta$  could be useful for some ultrasound systems in which a small degradation in image quality is acceptable so that the computational load during the DRBF can be significantly reduced [9], [20].

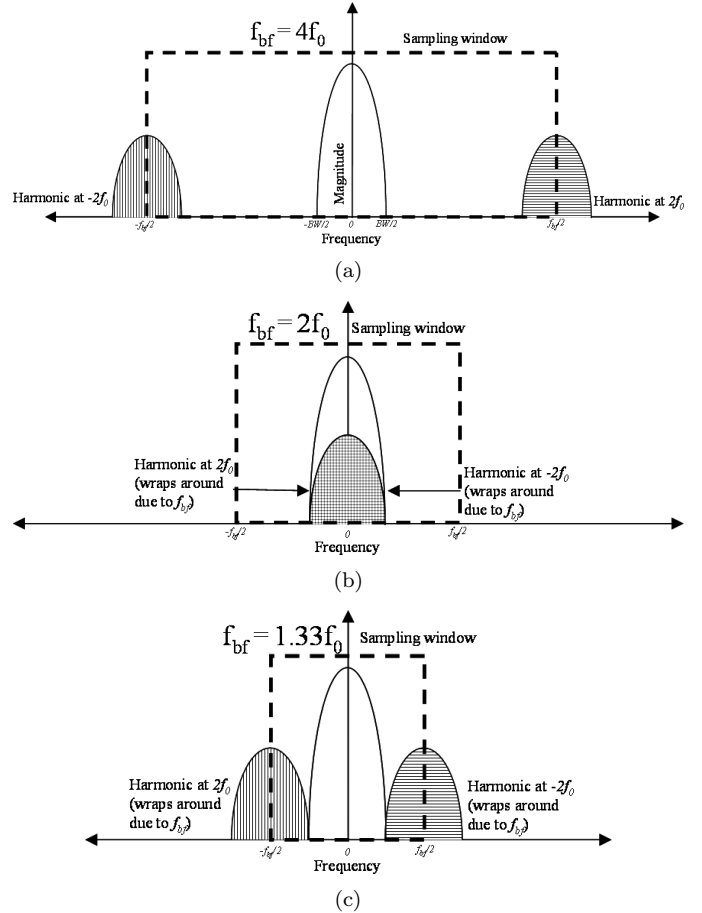


Fig. 14. Frequency spectrum of the in-phase component of the beamformed signal in the TSD-based PRBF when the  $f_{bf}$  is (a)  $4f_0$ , (b)  $2f_0$ , and (c)  $1.33f_0$ .

### C. Computational Requirement of the QD- and TSD-Based PRBF

Table III lists the computational requirement of each processing function in the QD- and TSD-based PRBF in terms of multiplications and additions. It is found that the TSD significantly reduces the number of multiplications and additions needed for demodulation filtering in the PRBF. For example, when  $\eta$  is 1, the number of multiplications needed to support demodulation filtering in the PRBF with the TSD is 131,072 compared to 4,194,304 in the PRBF with the QD. As listed in Table III, this savings in demodulation filtering facilitates an overall reduction in the number of multiplications and additions for the PRBF by 84.9% and 88.2%, respectively. Fig. 16 shows the total number of multiplications and additions needed for the QD- and TSD-based PRBF as a function of  $\eta$ . As shown in Fig. 16, the TSD-based PRBF operating at  $\eta$  of 1 requires less number of operations than the QD-based PRBF operating at  $\eta = 4$  (i.e., 42.1% less multiplications and 52.6% less additions). Reducing the beamforming frequency in the TSD-based PRBF (i.e.,  $\eta > 1$ ) further increases the hardware savings with the proposed method. For example, when  $\eta$  is 3 in the TSD-based PRBF, the number

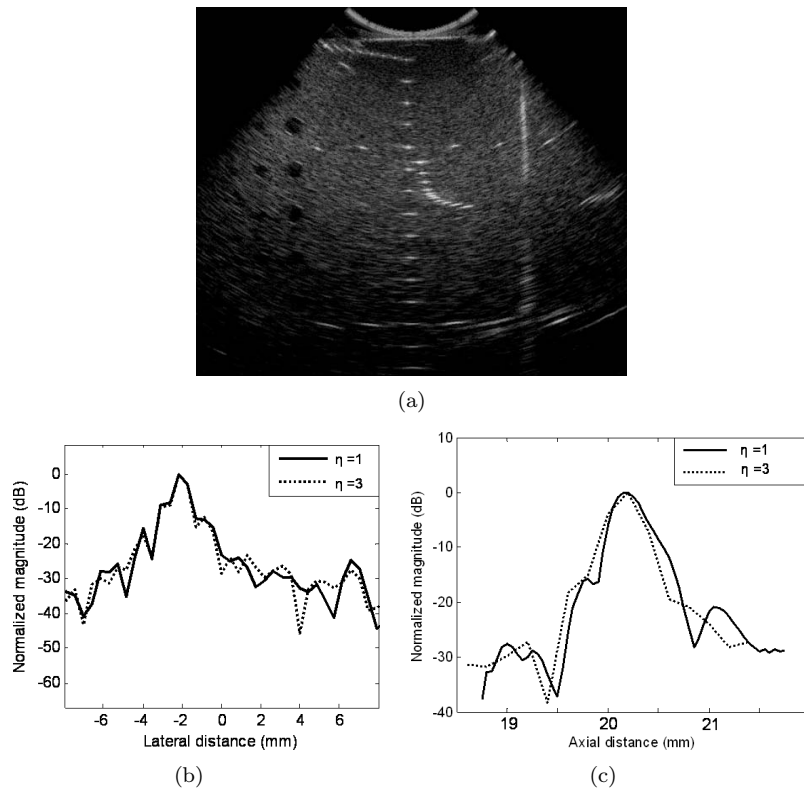


Fig. 15. Phantom study results with 60 dB dynamic range. (a) Ultrasound image with TSD-based PRBF at  $\eta$  of 3. (b) Lateral and (c) axial resolution of the TSD-based PRBF at the imaging depth of 20 mm when  $\eta$  is 1 and 3.

TABLE III  
MULTIPLICATIONS AND ADDITIONS REQUIREMENTS.<sup>1</sup>

Function	QD-based PRBF		TSD-based PRBF	
	Multiplications	Additions	Multiplications	Additions
Mixing	$\frac{KM}{2}$	—	$\frac{KM}{2}$	—
Demodulation filter	$\frac{2JKM}{\eta}$	$\frac{2(J-1)KM}{\eta}$	$\frac{2JM}{\eta}$	$\frac{2(J-1)M}{\eta}$
Phase compensation	$\frac{4KM}{\eta}$	$\frac{2KM}{\eta}$	$\frac{4KM}{\eta}$	$\frac{2KM}{\eta}$
Sum	—	$\frac{(K-1)M}{\eta}$	—	$\frac{(K-1)M}{\eta}$
Total	4,784,128	4,321,280	720,896	512,000

<sup>1</sup>Required for various functions in the QD- and TSD-based PRBF to generate one scanline data based on the number of channels ( $K$ ), the filter tap size ( $J$ ), the number of ADC samples per scanlines ( $M$ ) and the ratio of ADC sampling frequency to beamforming frequency ( $\eta$ ). The total number of operations is listed for  $K = 32$ ,  $J = 16$ ,  $M = 4096$ , and  $\eta = 1$ .

of multiplications and additions can be reduced by 82.7% and 88.2%, respectively, compared to the QD-based PRBF operating at  $\eta$  of 3.

The selection of  $\eta$  in the proposed TSD-based PRBF determines both the computational requirement and the image quality. The proposed method with  $\eta$  of 1 could be used to facilitate the development of high-channel count systems in which the reduction in the computational complexity of receive beamforming without compromising the image quality is critical (e.g., 3-D beamforming for a 2-D array transducer with hundreds or thousands of elements).

However, the TSD-based PRBF with  $\eta > 1$  (e.g.,  $\eta$  of 3) could be beneficial to the development of low-end ultrasound systems in which significant reduction in the cost, size, and power requirements is needed, and a small degradation in image quality would be tolerable. These low-cost ultrasound systems have the potential to facilitate more widespread use of ultrasound technology in local clinics (e.g., used in screening the patients by the general practitioners [21], [22]) and/or in remote patient management in distributed diagnosis and home healthcare environments [20], [23], [24].

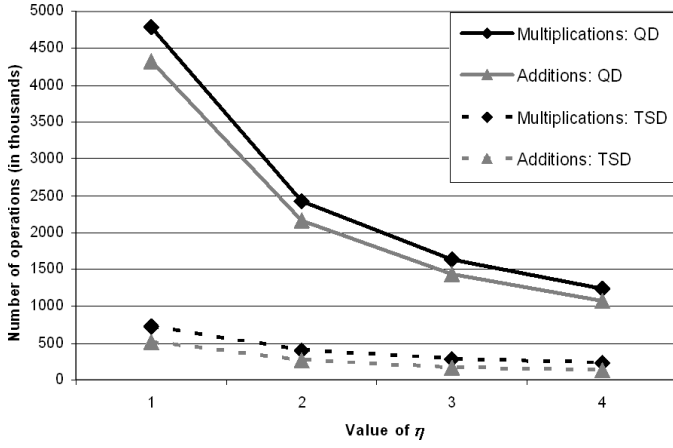


Fig. 16. Total number of multiplications and additions needed to support the QD- and TSD-based PRBF.

## V. CONCLUSIONS

In this paper, the new two-stage demodulation method has been presented. Although significantly reducing the hardware complexity compared to the commonly-used QD, the developed method could suffer from image artifacts due to nonlinearity in dynamic focusing leading to sample selection error during demodulation, and signal aliasing due to the presence of harmonics during beamforming. From simulation and phantom studies, the SSE in the developed method has been found to have a negligible impact on the image quality in terms of spatial and contrast resolution. Upon reducing the beamforming frequency, however, further hardware reduction is possible at the cost of small degradation in image quality. Thus, the two-stage demodulation method would be useful in supporting the image quality requirement in large-channel count systems (e.g., 3-D) as well as reduced complexity requirement in low-end (e.g., portable) ultrasound systems by controlling the beamforming frequency used during phase-rotation-based-beamforming.

## APPENDIX A

### A. Output Expression with the QD-Based PRBF

Assuming the RF signal as given in (1), the in-phase and quadrature components after mixing for the  $k^{\text{th}}$  channel are given by:

$$\begin{aligned} B_k^i[m] &= u_k[m] \cos[\omega_0 m] \\ &= \frac{1}{2} (A_k^i[m] + A_k^i[m] \cos[2\omega_0 m] - A_k^q[m] \sin[2\omega_0 m]), \end{aligned} \quad (\text{A1})$$

$$\begin{aligned} B_k^q[m] &= u_k[m] \sin[\omega_0 m] \\ &= \frac{1}{2} (-A_k^q[m] + A_k^i[m] \sin[2\omega_0 m] \\ &\quad + A_k^q[m] \cos[2\omega_0 m]). \end{aligned} \quad (\text{A2})$$

The mixed signal contains harmonics at  $\pm 2f_0$  in addition to the baseband component. These harmonics can be

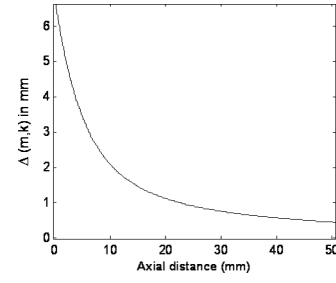


Fig. A1.  $\Delta(m, k)$  as a function of the imaging distance for the outermost channel of a 32 element linear array transducer.

removed by applying a lowpass filter. The outputs after lowpass filtering are given by:

$$C_k^i[m] = \sum_{j=-J/2}^{J/2-1} a_j B_k^i[m+j] = \sum_{j=-J/2}^{J/2-1} \frac{a_j A_k^i[m+j]}{2}, \quad (\text{A3})$$

$$C_k^q[m] = \sum_{j=-J/2}^{J/2-1} a_j B_k^q[m+j] = - \sum_{j=-J/2}^{J/2-1} \frac{a_j A_k^q[m+j]}{2}, \quad (\text{A4})$$

where  $J$  is the filter tap size and  $a_j$  is the filter coefficient for the  $j^{\text{th}}$  filter tap. Dynamic focusing is performed for coherent summation of signals from various channels. To achieve focusing at the  $l^{\text{th}}$  sample, the  $[m + \Delta[m, k]]^{\text{th}}$  complex baseband sample is selected, where  $m$  is  $\eta l$ ,  $l$  varies from 1 to  $L$ ,  $L$  is the number of beamformed samples per scanline, and  $\Delta[m, k]$  is the dynamic focusing delay applied to account for the delay difference between the  $k^{\text{th}}$  receive channel element and the center element. The delayed complex baseband samples are phase rotated prior to summation across the channels [13], [14]. The output obtained after phase rotation and summation across the  $k$  channels are given by:

$$Z^i[l] = \sum_{k=-K/2}^{K/2-1} b_k \begin{bmatrix} C_k^i[m + \Delta[m, k]] \cos[\omega_0 \Delta[m, k]] \\ -C_k^q[m + \Delta[m, k]] \sin[\omega_0 \Delta[m, k]] \end{bmatrix} \quad l = 1, 2, \dots, L, \quad (\text{A5})$$

$$Z^q[l] = \sum_{k=-K/2}^{K/2-1} b_k \begin{bmatrix} C_k^i[m + \Delta[m, k]] \sin[\omega_0 \Delta[m, k]] \\ +C_k^q[m + \Delta[m, k]] \cos[\omega_0 \Delta[m, k]] \end{bmatrix} \quad l = 1, 2, \dots, L, \quad (\text{A6})$$

where  $b_k$  is the apodization coefficient for the  $k^{\text{th}}$  channel. Eq. (A5) and (A6) can be rewritten as:

$$\begin{aligned} Z^i[l] &= \sum_{k=-K/2}^{K/2-1} b_k \sum_{j=-J/2}^{J/2-1} \frac{a_j}{2} \\ &\quad \times \begin{bmatrix} A_k^i[m+j+\Delta[m, k]] \cos[\omega_0 \Delta[m, k]] \\ +A_k^q[m+j+\Delta[m, k]] \sin[\omega_0 \Delta[m, k]] \end{bmatrix}, \end{aligned} \quad (\text{A7})$$

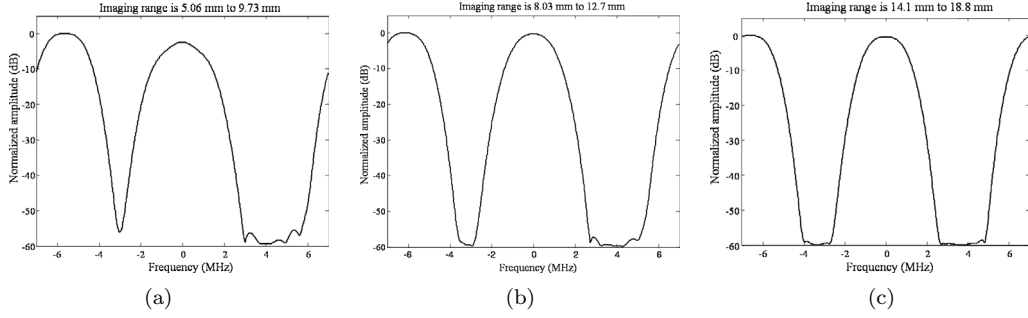


Fig. A2. Frequency spectrum of the phase compensated signal for the outermost channel at the imaging depths of (a) 5 mm, (b) 10 mm, and (c) 15 mm.

$$Z^q[l] = \sum_{k=-K/2}^{K/2-1} b_k \sum_{j=-J/2}^{J/2-1} \frac{a_j}{2} \times \begin{bmatrix} A_k^i[m+j+\Delta[m,k]] \sin[\omega_0 \Delta[m,k]] \\ -A_k^q[m+j+\Delta[m,k]] \cos[\omega_0 \Delta[m,k]] \end{bmatrix} \quad (\text{A8})$$

Because  $\Delta[m, k]$  is not restricted to integer values, the samples required for receive focusing at various depths do not fall exactly on the uniform sampled data ((A7) and (A8)). Ideally, interpolation needs to be performed to obtain the sample values, but it is typically not performed, resulting in a time quantization error. This error is considered negligible because a slowly varying baseband signal is sampled [13], [14].

### B. Output Expression with the TSD-Based PRBF

Assuming the same quantized RF data as expressed in (1), the output signals after phase rotation beamforming (i.e., dynamic delay, phase rotation, and summation) with the proposed two-stage demodulation are given by:

$$C^i[l] = \sum_{k=-K/2}^{K/2-1} b_k \begin{bmatrix} A_k^i[m+\Delta[m,k]] \cos[\omega_0 \Delta[m,k]] \\ +A_k^q[m+\Delta[m,k]] \sin[\omega_0 \Delta[m,k]] \\ +A_k^i[m+\Delta[m,k]] \cos[2\omega_0 m + 3\omega_0 \Delta[m,k]] \\ -A_k^q[m+\Delta[m,k]] \sin[2\omega_0 m + 3\omega_0 \Delta[m,k]] \end{bmatrix}, \quad (\text{A9})$$

$$C^q[l] = \sum_{k=-K/2}^{K/2-1} b_k \times \begin{bmatrix} A_k^i[m+\Delta[m,k]] \sin[\omega_0 \Delta[m,k]] \\ -A_k^q[m+\Delta[m,k]] \cos[\omega_0 \Delta[m,k]] \\ +A_k^i[m+\Delta[m,k]] \sin[2\omega_0 m + 3\omega_0 \Delta[m,k]] \\ +A_k^q[m+\Delta[m,k]] \cos[2\omega_0 m + 3\omega_0 \Delta[m,k]] \end{bmatrix}. \quad (\text{A10})$$

Thus, in addition to the baseband component, there is a signal component at the frequency of  $[\pm 2\omega_0 m + 3\omega_0 \Delta[m, k]]$ . The impact of an additional frequency term (i.e.,  $3\omega_0 \Delta[m, k]$ ) at  $\pm 2f_0$  depends on the magnitude and rate of change of  $\Delta[m, k]$  as a function of axial distance (i.e.,  $m$ ). For example, if  $\Delta[m, k]$  is constant with depth, it only will introduce a phase shift in the harmonic centered at  $\pm 2f_0$ . As shown in Fig. A1 for the outermost channel of a 32-channel linear array transducer,  $\Delta[m, k]$  decreases

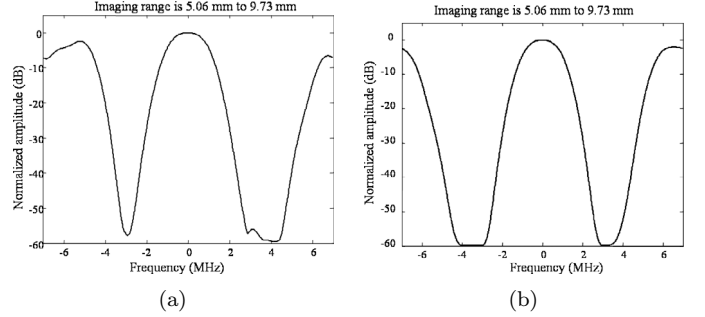


Fig. A3. Frequency spectrum of the summation signal in the TSD-based PRBF at the imaging depth of 5 mm (a) without dynamic aperture and (b) when dynamic aperture with  $f$ -number of 1.

exponentially with imaging distance. Thus, the effect of the additional frequency component decreases as the imaging distance increases. Fig. A2 shows the frequency spectrum of the phase-compensated signal in the TSD-based PRBF for the outermost channel (i.e., complex signal before summation) as the imaging depth is increased from 5 mm to 15 mm when the received signal is modeled as a sine-modulated Gaussian signal with  $\text{BW} = 1.4f_0$  and  $f_{\text{bf}} = 4f_0$ . As shown in Fig. A2, the additional frequency term causes a shift in the harmonics, and this shift is reduced as the imaging depth increases. Furthermore, the baseband component still can be recovered from this signal at various imaging depths. Fig. A3(a) shows the summation signal (i.e.,  $C^i[l] + jC^q[l]$ ) for the imaging depth of 5 mm.

As shown in Fig. A3(a), the summation of the signals from various channels reduces the frequency shift in the signal harmonics. The frequency shift can be further reduced by using dynamic aperture during receive beamforming as shown in Fig. A3(b), which shows the result with  $f$ -number = 1. Similar results also are obtained for other transducer configurations. Thus, the signal component at  $[\pm 2\omega_0 m + 3\omega_0 \Delta[m, k]]$  can be removed by lowpass filtering, and the signal after lowpass filtering is given by:

$$Z^i[l] = \sum_{k=-K/2}^{K/2-1} b_k \sum_{j=-J/2}^{J/2-1} \frac{a_j}{2} \times \begin{bmatrix} A_k^i[m+\eta j+\Delta[m+\eta j,k]] \cos[\omega_0 \Delta[m+\eta j,k]] \\ +A_k^q[m+\eta j+\Delta[m+\eta j,k]] \sin[\omega_0 \Delta[m+\eta j,k]] \end{bmatrix}, \quad (\text{A11})$$

$$\begin{aligned}
 Z^q[l] &= \sum_{k=-K/2}^{K/2-1} b_k \sum_{j=-J/2}^{J/2-1} \frac{a_j}{2} \\
 &\times \begin{bmatrix} A_k^i[m + \eta j + \Delta[m + \eta j, k]] \sin[\omega_0 \Delta[m + \eta j, k]] \\ -A_k^q[m + \eta j + \Delta[m + \eta j, k]] \cos \omega_0 \Delta[m + \eta j, k]] \end{bmatrix}.
 \end{aligned} \tag{A12}$$

As seen by comparing (A7) and (A11), incorrect samples are selected during demodulation filtering in the TSD compared to the QD (i.e., samples based on  $(m + \eta j + \Delta[m + \eta j, k])$  are selected in the TSD as opposed to  $(m + j + \Delta[m, k])$  in the QD). A potential TSD SSE component,  $(\eta - 1)j$ , is due to downsampling of the input signal during lowpass filtering in the TSD-based PRBF when  $\eta > 1$ . In the absence of aliasing in the downsampled signal, this will not introduce any signal degradation if the lowpass filter coefficients ( $a_j$ ) are updated with changing values of  $\eta$  [15]. However, the SSE component due to the nonlinear nature of dynamic focusing can introduce signal degradation and is given by:

$$\text{SSE}(m, j, k, \eta) = \Delta[m, k] - \Delta[m + \eta j, k]. \tag{A13}$$

## REFERENCES

- [1] S. Stergiopoulos, *Advanced Signal Processing Handbook: Theory and Implementation for Radar, Sonar, and Medical Imaging Real Time Systems*. Boca Raton, FL: CRC Press, 2000, pp. 2–30.
- [2] B. D. Steinberg, “Digital beamforming in ultrasound,” *IEEE Trans. Ultrason., Ferroelect., Freq. Contr.*, vol. 39, pp. 716–721, 1992.
- [3] J. N. Wright, C. R. Cole, and A. Gee, “Method and apparatus for a baseband processor for a receive beamformer system,” U. S. Patent No. 5,928,152, Jul. 27, 1999.
- [4] M. O’Donnell, W. E. Engeler, J. J. Bloomer, and J. T. Pedicone, “Method and apparatus for digital phase array imaging,” U. S. Patent No. 4,983,970, Jan. 8, 1991.
- [5] S. R. Freeman, M. K. Quick, M. A. Morin, R. C. Anderson, C. S. Desilets, T. E. Linnenbrink, and M. O’Donnell, “Delta-sigma oversampled ultrasound beamformer with dynamic delays,” *IEEE Trans. Ultrason., Ferroelect., Freq. Contr.*, vol. 46, pp. 320–332, 1999.
- [6] A. Fenster and D. B. Downey, “3D ultrasound imaging: A review,” *IEEE Eng. Med. Biol.*, vol. 15, no. 6, pp. 41–51, 1996.
- [7] J. Kellett, “Ultrasound in the palm of your hand: The dawn of a new golden age of bedside medicine,” *Eur. J. Internal Med.*, vol. 15, pp. 335–336, 2004.
- [8] J. H. Kim, T. K. Song, and S. B. Park, “A pipelined sampled delay focusing in ultrasound imaging systems,” *Ultrason. Imag.*, vol. 9, pp. 75–91, 1987.
- [9] K. Ranganathan, M. K. Santy, T. N. Blalock, J. A. Hossack, and W. F. Walker, “Direct sampled I/Q beamforming for compact and very low-cost ultrasound imaging,” *IEEE Trans. Ultrason., Ferroelect., Freq. Contr.*, vol. 51, pp. 1082–1094, 2004.
- [10] S. H. Chang, K. I. Jeon, M. H. Bae, and S. B. Park, “Sampling-point-wise digital dynamic focusing in the receive mode of an ultrasonic linear array imaging system,” in *Proc. IEEE Ultrason. Symp.*, 1993, pp. 1163–1165.
- [11] S. E. Noujaim, S. L. Garverick, and M. O’Donnell, “Phased array ultrasonic beam forming using oversampled A/D converters,” U. S. Patent 5,203,335, Apr. 20, 1993.
- [12] M. Kozak and M. Karaman, “Digital phased array beamforming using single-bit delta-sigma conversion with non-uniform oversampling,” *IEEE Trans. Ultrason., Ferroelect., Freq. Contr.*, vol. 48, pp. 922–931, 2001.
- [13] S. H. Chang, S. B. Park, and G. H. Cho, “Phase-error-free quadrature sampling technique in the ultrasonic B-scan imaging system and its application to the synthetic focusing system,” *IEEE Trans. Ultrason., Ferroelect., Freq. Contr.*, vol. 40, pp. 216–223, 1993.
- [14] D. C. M. Horvat, J. S. Bird, and M. M. Goulding, “True time-delay bandpass beamforming,” *IEEE J. Oceanic Eng.*, vol. 17, pp. 185–192, 1992.
- [15] A. V. Oppenheim, R. W. Schaffer, and J. R. Buck, *Discrete-Time Signal Processing*. 2nd ed. Upper Saddle River, NJ: Prentice-Hall, 1998, pp. 140–158.
- [16] R. T. Bjerngaard and J. A. Jensen, “Should compression of coded waveforms be done before or after focusing?,” *Proc. SPIE: Progress Biomed. Opt. Imaging*, vol. 4687, pp. 47–58, 2002.
- [17] H. Susaki, “A fast algorithm for high-accuracy frequency measurement: Application to ultrasonic Doppler sonar,” *IEEE J. Oceanic Eng.*, vol. 27, pp. 5–12, 2002.
- [18] J. A. Jensen, “Field: A program for simulating ultrasound systems,” *Med. Biol. Eng. Comput.*, vol. 34, pp. 351–353, 1996.
- [19] K. L. Gammelmark and J. A. Jensen, “Multielement synthetic transmit aperture imaging using temporal encoding,” *IEEE Trans. Med. Imag.*, vol. 22, pp. 552–563, 2003.
- [20] Y. M. Yoo, F. K. Schneider, A. Agarwal, T. Fukuoka, L. M. Koh, and Y. Kim, “Ultrasound machine for distributed diagnosis and home use,” in *Transdisciplinary Conference on Distributed Diagnosis and Home Healthcare*, 2006, pp. 63–66.
- [21] E. C. Vourvouri, D. Poldermans, A. F. L. Schinkel, F. B. Sozzi, J. J. Bax, H. van Urk, and J. R. T. C. Roelandt, “Abdominal aortic aneurysm screening using a hand-held ultrasound device. A pilot study,” *Eur. J. Vasc. Endovasc. Surg.*, vol. 22, pp. 352–354, 2001.
- [22] A. Karavidas, E. Matsakas, and G. Lazaros, “Emergency bedside echocardiography as a tool for early detection and clinical decision making in cases of suspected pulmonary embolism: A case report,” *Angiology*, vol. 51, pp. 1021–1025, 2000.
- [23] E. H. Kim, J. J. Kim, F. A. Matsen, III, and Y. Kim, “Distributed diagnosis and home healthcare (D<sub>2</sub>H<sub>2</sub>) and patient-centered electronic medical record,” in *Proc. 1st Int. Bioeng. Conf.*, 2004, pp. 461–468.
- [24] Y. Kim, “Electronic house calls: High-tech medicine at your doorstep,” in *Proc. 26th Annu. Int. Conf. IEEE EMBS*, 2004, p. 5216.



**Anup Agarwal** received the B.Tech. (Hons.) degree in electronics and electrical communications from the Indian Institute of Technology, Kharagpur, India, in 2000 and the M.S. degree in electrical engineering from the University of Washington, Seattle, WA, in 2002, where he is currently pursuing the Ph.D. degree in electrical engineering. He has been working on novel front-end algorithms and architecture to enable a low-cost hand-held portable ultrasound machine. His interests include medical imaging, compression techniques, and high performance processors architectures and programming.

niques, and high performance processors architectures and programming.

**Yang Mo Yoo** received the Bachelor and Master of Science degrees of Electronic Engineering in 1999 and 2001, respectively, at the Sogang University, Seoul, Korea. He is currently working towards the Ph.D. degree in Bioengineering at the University of Washington, Seattle, WA. He has been researching and developing a hand-held ultrasound machine that would allow clinicians to have access to patients remotely and be able to quickly make diagnostic decision. Also, he has been working for developing real-time 3-D color Doppler imaging where 3-D anatomical structures are integrated with flow information. His research interests include digital signal processing, system design, and high-performance computing architecture for medical imaging and its applications.



**Fabio Kurt Schneider** received the B.S. in Electrical Engineering and the M.Sc. in Biomedical Engineering in 1989 and 1995, respectively, both from Federal Technological University of Parana, Parana, Brazil. He received his Ph.D. from the University of Washington in Electrical Engineering in 2006. Since 1995, he has been with the Federal Technological University of Parana in the Academic Department of Electronics. In addition to teaching and researching, he has been involved in development activities with industry since

1989. His research interests have been in areas including biomedical signal and image processing, ultrasound imaging, bioinstrumentation, digital systems design based on high-performance digital signal processors, reconfigurable devices, and ASICs.

**Changqing Gao** was born in August 1980, China. He received the B.Sc. degree in Electrical Engineering from Nanjing University, Nanjing, China in June 2002. He is currently working towards Ph.D. degree in Nanyang Technological University, Singapore. His research work primarily concerns with low cost digital beamforming for medical ultrasound imaging.

**Liang Mong Koh** No bio available.



**Yongmin Kim** (S'79–M'82–SM'87–F'96) received the B.S. degree in electronics engineering from Seoul National University, Seoul, Korea, and the M.S. and Ph.D. degrees in electrical engineering from the University of Wisconsin, Madison, WI.

He is the Hunter and Dorothy Simpson Endowed Chair in Bioengineering, Professor and Chair of Bioengineering, Professor of Electrical Engineering, and Adjunct Professor of Radiology, and Computer Science and Engineering at the University of Washington, Seattle,

WA. His research interests are in distributed diagnosis and home healthcare, medical imaging, algorithms and systems for multimedia, image processing, high-performance programmable processor architecture, and modeling and simulation. He has more than 380 publications and his group has 72 patents and 22 commercial licenses.

Dr. Kim received the Early Career Achievement Award from the IEEE Engineering in Medicine and Biology Society (EMBS) in 1988 and the 2003 Ho-Am Prize in Engineering. He is a Member of the Editorial Board of the *Proceedings of the IEEE*, *IEEE Transactions on Biomedical Engineering*, and *IEEE Transactions on Information Technology in Biomedicine*. He was the President-Elect of the IEEE EMBS in 2004.